



Roles of bulk $\gamma(\text{L})\text{-Bi}_2\text{MoO}_6$ and surface $\beta\text{-Bi}_2\text{Mo}_2\text{O}_9$ in the selective catalytic oxidation of C_3H_6

Takehiko Ono^{a,*}, Kazuya Utsumi^a, Satoshi Tsukamoto^a, Hiroyuki Tamaru^a, Masakazu Kataoka^a, Fumio Noguchi^b

^a Department of Environmental Science and Technology, Faculty of Engineering, Shinshu University, 4-17-1 Wakasato, Nagano 380-8553, Japan

^b Department of Applied Chemistry, Faculty of Engineering, Saitama University, 255 Shimo-ookawa, Saitama 338-8570, Japan

ARTICLE INFO

Article history:

Received 24 August 2009

Received in revised form

20 November 2009

Accepted 21 November 2009

Available online 27 November 2009

Keywords:

$\gamma(\text{L})\text{-Bi}_2\text{MoO}_6$

Propene oxidation

UV–vis spectra of Bi–Mo oxides

Crystal structure visualization of Bi–Mo oxides

Rapid oxygen transfer

ABSTRACT

$\gamma(\text{L})\text{-Bi}_2\text{MoO}_6$ (L: low temperature phase) catalysts, whose surface compositions have a Mo/Bi ratio above = 0.5, exhibited high selectivity in the partial oxidation of C_3H_6 , while catalysts with Mo/Bi surface ratios near or below = 0.5 exhibited low selectivity. $\gamma(\text{L})$ -phase catalysts which have Mo/Bi surface ratios greater than = 0.5, were demonstrated to form $\beta\text{-Bi}_2\text{Mo}_2\text{O}_9$ on their surface. An interaction between the β - and $\gamma(\text{L})$ -phases was observed in these catalysts' UV–vis spectra at 430 nm. The new β -phase material seems to grow along *b*-axis of $\gamma(\text{L})$ -phase, i.e., perpendicular to $\text{MoO}_2\text{-Bi}_2\text{O}_2$ layers. Structure visualizations revealed that the $\alpha\text{-Bi}_2\text{Mo}_3\text{O}_{12}$, β -, and $\gamma(\text{H})$ -phases, which are selective catalysts, contain twin Mo tetrahedral structures, and that their Mo and Bi ions lie on the same plane. The pure $\gamma(\text{L})$ -phase does not contain this structure. A model for the very rapid transfer of oxygen between the $\gamma(\text{L})$ - and β -phases is discussed in relation to the kinetics of C_3H_6 oxidation.

© 2009 Elsevier B.V. All rights reserved.

1. Introduction

It is well known that $\alpha\text{-Bi}_2\text{Mo}_3\text{O}_{12}$, $\beta\text{-Bi}_2\text{Mo}_2\text{O}_9$, and $\gamma\text{-Bi}_2\text{MoO}_6$ are highly selective catalysts for the partial oxidation of C_3H_6 [1,2]. However, the selectivity of pure $\gamma(\text{L})\text{-Bi}_2\text{MoO}_6$ (L = low temperature phase) remains an area of a debate. Matsuura et al. [3] have previously reported that pure $\gamma(\text{L})$ -phase material displays poor activity and selectivity in the oxidation of butene. However, recent reports have shown that $\gamma(\text{L})\text{-Bi}_2\text{MoO}_6$ exhibits high activity and selectivity in the partial oxidation of olefins [4–6]. Well et al. have recently reported that the activities of Bi_2MoO_6 catalysts that are used for the selective oxidation of C_3H_6 that contain a small excess of bismuth are strongly dependent on the calcination conditions used in their preparation [7]. Soares et al. have reported a synergistic effects using the β - and γ -phases for the selective oxidation of 1-butene [8]. Buttrey et al. previously reported a connection between the structure of fluolite and bismuth molybdate catalysts used in selective oxidation [9], and suggested that the structure of the γ -phase's surface, which is present during catalysis, should be re-examined [10].

It is important to study the roles of the $\gamma(\text{L})$ -phase and the surface β -phase in the catalytic partial oxidation of C_3H_6 . In the

present report, the selectivities of $\gamma(\text{L})$ -phase catalysts, which were prepared by various methods such that they had Mo/Bi = 0.5, and of $\gamma(\text{H})\text{-Bi}_2\text{MoO}_6$ (H = high temperature phase) catalysts for the oxidation of C_3H_6 were studied. After the $\gamma(\text{L})$ -phase catalysts had been combined with a small amount of MoO_3 , the modified catalysts' activity and selectivity in the oxidation of C_3H_6 were re-examined [3]. The roles of the surface Bi–Mo species and of the bulk pure $\gamma(\text{L})$ -phase in these catalysts were studied by characterizing them spectroscopically. Using crystal structure visualizations, we previously reported that α -, β -, and $\gamma(\text{H})$ -phase catalysts bear twin Mo tetrahedral structures, and that their Mo and Bi ions lie in the same plane [11]. Such structures are compared to those of the pure $\gamma(\text{L})$ -phase catalysts in this work. The active sites of the Mo rich $\gamma(\text{L})$ -phase catalysts, into which oxygen atoms were inserted from gaseous dioxygen, were studied using an $^{18}\text{O}_2$ tracer previously [12]. In accord with previous ^{18}O tracer studies and kinetic studies carried out by other researchers, a modified redox model for Mo rich $\gamma(\text{L})$ -phase catalyst is also discussed in this work.

2. Experimental

2.1. Catalyst preparation

The $\gamma(\text{L})$ -phase (A) (Mo/Bi = 0.5) catalyst was prepared using the procedure of Batist et al. [13]. $\text{Bi}(\text{NO}_3)_3 \cdot 5\text{H}_2\text{O}$ (7.95 g, Wako,

* Corresponding author. Tel.: +81 26 293 5831; fax: +81 26 269 5550.
E-mail address: takeono@shinshu-u.ac.jp (T. Ono).

Japan) was dissolved in aqueous nitric acid (20 ml) (solution I). $(\text{NH}_3)_6\text{Mo}_7\text{O}_{24}\cdot 4\text{H}_2\text{O}$ (1.44 g, Wako, Japan) was dissolved in aqueous ammonia (15 ml) (solution II). Solutions (I) and (II) were mixed together and adjusted to pH 7 by the addition of aqueous ammonia. The mixture was concentrated to dryness, and then heated at 500 °C for 12 h. The $\gamma(\text{L})$ -phase (B) ($\text{Mo}/\text{Bi}=0.5$) catalyst was prepared by dissolving $\text{Bi}(\text{NO}_3)_3\cdot 5\text{H}_2\text{O}$ (7.95 g) and $(\text{NH}_3)_6\text{Mo}_7\text{O}_{24}\cdot 4\text{H}_2\text{O}$ (1.44 g) in distilled water, and allowing the solution to evaporate to dryness open to the air. The resulting solid was heated at 500 °C for 6 h. In this case, the $\gamma(\text{L})$ - Bi_2MoO_6 (B) catalysts were prepared with a range of Mo contents from deficient to excessive. These catalysts are denoted as (B). The $\gamma(\text{L})$ -phase (C) catalysts containing excess MoO_3 were prepared by a solid state mixing method. The solid state mixing method involved mixing the requisite amount of pure $\gamma(\text{L})$ -phase and powdered MoO_3 at 2, 4, and 6 wt% and heating the mixture at 500 °C for 6 h. These catalysts are denoted as (C). The $\gamma(\text{H})$ -phase catalyst was prepared by heating the $\gamma(\text{L})$ -phase (B) catalyst at 800 °C for 6 h.

2.2. Catalyst characterization

Catalysts were characterized using XRD, XPS, LRS, and UV–vis spectra. XRD results were obtained using a Lab X XRD-6000 (SHIMADZU) diffractometer. Laser Raman spectra were recorded using a JRS-system1000 (Reinshaw Raman) spectrometer. UV–vis spectra were recorded using a UV-3150 (SHIMADZU) spectrometer. The surface areas of the Bi–Mo oxides, when prepared as described above, generally ranged from 1 to 3 m^2/g for the preparation and were not determined in this work.

The surface composition with respect to Bi and Mo ions was determined by XPS techniques using an ESCA 5600 (Albac) and an S-Probe ESCA (Surface Science Instruments) with an Al $K\alpha$ radiation source. An example of a XPS wide spectra of a Bi–Mo oxide catalyst ($\gamma(\text{H})$ - Bi_2MoO_6) is shown in Fig. 1. In the cases of the $\gamma(\text{L})$ -phase catalysts (as described below in Table 1 of Section 3.1), $\text{Mo}3\text{P}3$ and $\text{Bi}4\text{f}7$ peaks were used to obtain Mo/Bi ratio. For the $\gamma(\text{H})$ -phase and the $\gamma(\text{L})$ -phase (C) catalysts, narrow spectra of the $\text{Bi}4\text{f}5$ and $4\text{f}7$ peaks, as well as spectra of the $\text{Mo}3\text{d}3$ and $3\text{d}5$ peaks, were measured in addition to obtaining the wide spectra. Peak areas were determined by computerized peak shape analysis and used along with sensitivity factors to determine the Mo/Bi ratios (as described later in Tables 2 and 3 in Sections 3.1 and 3.2). The experimental errors in Mo/Bi ratios were $\pm 10\%$ when double peaks were used in the XPS method. The errors were below $\pm 10\%$ when a single peak was used.

Table 1

Selectivity for acrolein production in C_3H_6 oxidation over $\gamma(\text{L})$ - Bi_2MoO_6 catalysts in the absence of dioxygen and the catalysts' Mo/Bi ratio as determined by XPS methods.

| Reaction time | Acrolein selectivity (%) | Propene conversion (%) | Signal | XPS atom (%) | Mo/Bi |
|---|--------------------------|------------------------|--|----------------|-------|
| $\gamma(\text{L})$ - Bi_2MoO_6 -(A) | 80 | 2.3 | $\text{Bi}4\text{f}7$ $\text{Mo}3\text{p}3$ | 55 44 | 0.8 |
| $\gamma(\text{L})$ - Bi_2MoO_6 -(B) | 3 | 1.4 | $\text{Bi}4\text{f}7$ $\text{Mo}3\text{p}3$ | 68–67 32–33 | 0.48 |

Catalyst: 1 g, $P_{\text{C}_3\text{H}_6}$: 6–8 kPa, reaction temperature: 500 °C, reaction time: 5 min. (A) and (B) denote the catalyst preparation methods.

Table 2

Selectivity for acrolein production in C_3H_6 oxidation over $\gamma(\text{H})$ - Bi_2MoO_6 catalyst in the absence of dioxygen and catalysts' Mo/Bi ratio as determined by XPS method.

| Reaction time | Acrolein selectivity (%) | Propene conversion (%) | Signal | XPS atom (%) | Mo/Bi |
|---------------|--------------------------|------------------------|--|----------------|-----------|
| 10 min | 78 | 0.2 | $\text{Bi}4\text{f}$ $\text{Mo}3\text{d}$ | 68–65 32–35 | 0.47–0.54 |
| 20 min | 37 | 1.0 | | | |

Catalyst: 1 g, $P_{\text{C}_3\text{H}_6}$: 6 kPa, reaction temperature: 500 °C. XPS results are reported as the average value from three runs.

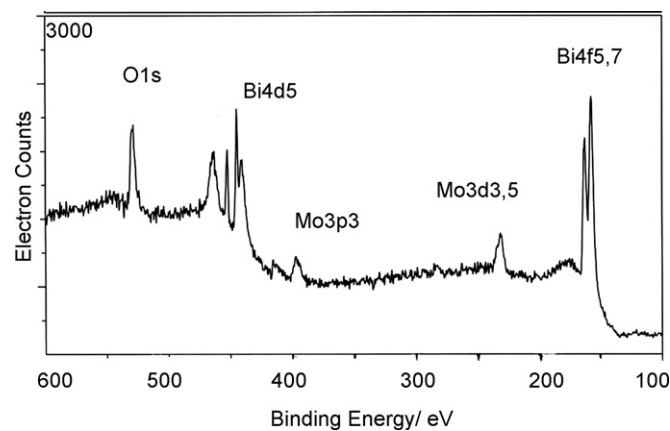


Fig. 1. An example of Bi–Mo oxide catalyst's ($\gamma(\text{H})$ - Bi_2MoO_6) XPS wide spectrum between 100 and 600 eV.

Table 3

Mo/Bi ratios of $\gamma(\text{L})$ - Bi_2MoO_6 -(C) catalysts by XPS methods.

| Catalyst | Atom% | | Mo/Bi |
|---|----------------------|----------------------|-------|
| | $\text{Bi}4\text{f}$ | $\text{Mo}3\text{d}$ | |
| $\gamma(\text{L})$ - Bi_2MoO_6 -(B) | 67–68 | 33–32 | 0.48 |
| (B)+ MoO_3 (2 wt%) | 60 | 40 | 0.67 |
| (B)+ MoO_3 (4 wt%) | 59 | 41 | 0.70 |
| (B)+ MoO_3 (6 wt%) | 58 | 42 | 0.72 |

The catalysts were heated at 500 °C for 6 h after solid state mixing (see Section 2.1).

2.3. Crystal structure visualizations

The unit cells of β -, $\gamma(\text{L})$ -, and $\gamma(\text{H})$ -Bi–Mo phases were visualized by using the application Dispcrystal (Noguchi). The application Dispcrystal [11] was developed using the space group method. Lattice constants for the β -, $\gamma(\text{L})$ - and $\gamma(\text{H})$ -phases and the values of the x, y, and z coordinates for all atoms are provided in the attached CIF data, i.e., crystal structure data [10,14,15]. This data provides visualizations of the Mo, Bi, and O ions on the display. If the coordinates of oxygen ions are omitted, the unit cells consist of only Mo and Bi ions. By rotating the unit cells on a display, one can visually determine which arrangements of Bi and Mo ions lie in or out of a given plane.

2.4. Reaction procedures

The oxidation of C_3H_6 in the absence of oxygen using a static reactor was carried out at $500^\circ C$ and at ca. 6 kPa of C_3H_6 . After a desired reaction time, the reactor was cooled quickly to stop the reaction. The amounts of acrolein and CO_2 produced were determined by TCD gas chromatography. PEG400 column was used for acrolein analysis and silica gel for CO_2 . The acrolein yields and its selectivities were obtained in carbon base since other products were not formed except H_2O .

3. Results and discussion

3.1. Partial oxidation of C_3H_6 over $\gamma(L)$ - Bi_2MoO_6 and $\gamma(H)$ - Bi_2MoO_6 and catalyst characterization

The oxidation of C_3H_6 in the absence of oxygen was carried out over the $\gamma(L)$ - Bi_2MoO_6 (A) and (B) catalysts. The results are shown in Table 1. The (A) catalyst exhibited high selectivity for acrolein formation (>80%), while the (B) catalyst exhibited low selectivity (<3%). XRD results indicated that both the (A) and (B) catalysts have the same crystal structures, which were assigned to that of koechlinite [14]. The (A) catalyst's Raman spectra displayed a small band at 889 cm^{-1} resulting from β - $Bi_2Mo_2O_9$, as well as bands from $\gamma(L)$ - Bi_2MoO_6 (Fig. 2) while the (B) catalyst exhibited only bands from $\gamma(L)$ - Bi_2MoO_6 though the data is not shown. The XPS results indicated that the Mo/Bi surface composition of the (A) catalyst is ca. 0.8, while that of the (B) catalyst is ca. 0.5 (Table 1). The high selectivity in the oxidation of C_3H_6 when using the $\gamma(L)$ (A) catalyst appears to originate from the enrichment in Mo ions and the presence of a surface β -phase, which was estimated by XPS and Raman spectroscopy. No enrichment of Mo at the surface occurred with the (B) catalyst. An enrichment of Mo for the (A) catalyst should occur during its preparation process since the as-prepared Mo/Bi is 0.5 in both (A) and (B) cases. These results indicate that pure $\gamma(L)$ - Bi_2MoO_6 (i.e., pure koechlinite) appears to have low selectivity for the oxidation of C_3H_6 to acrolein.

The $\gamma(H)$ - Bi_2MoO_6 catalyst exhibited approximately 80% selectivity in the partial oxidation of C_3H_6 (Table 2), but its selectivity decreased from 80 to 40% with reaction time. The $\gamma(H)$ -phase exhibited good selectivity for acrolein production. The catalytic activity over $\gamma(H)$ -phase catalyst is ca. 10 times smaller than that over $\gamma(L)$ -phase (A) and (B) catalyst (Tables 1 and 2). Such a difference should come from the difference of surface area since the $\gamma(H)$ -phase catalyst was obtained by heating the $\gamma(L)$ -phase (B) catalyst at $800^\circ C$. Fig. 3 shows an XRD image of the $\gamma(H)$ catalyst, which is in agreement with JCPDS 22-112. The $\gamma(H)$ -phase material's Raman spectra showed a strong band at 899 cm^{-1} and several weak bands at 884, 868, 828, and 774 cm^{-1} . Table 2 indicates that the surface ratio of Mo/Bi ranges from 0.47 to 0.54 before

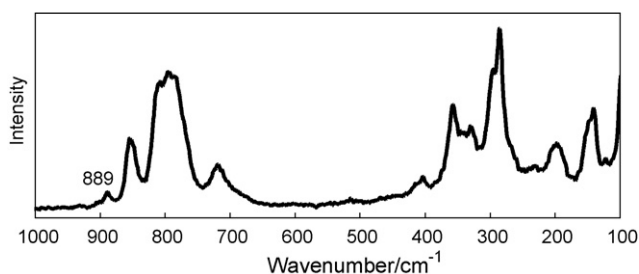


Fig. 2. Raman spectra of the $\gamma(L)$ - Bi_2MoO_6 catalysts which prepared by the (A) method as described in Section 2.1. The small band at 889 cm^{-1} is assigned to the β -phase material. All other bands were assigned to the $\gamma(L)$ -phase. The catalysts prepared by the (B) method exhibited Raman bands from the $\gamma(L)$ -phase only (not shown in the figure).

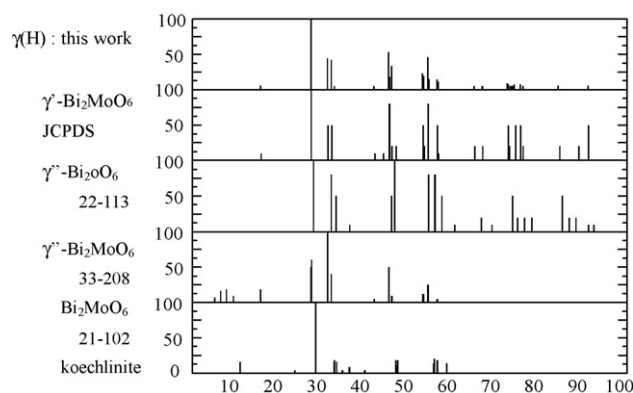


Fig. 3. XRD results from a $\gamma(H)$ Bi_2MoO_6 catalyst prepared and assignment with JCPDS cards.

the oxidation reactions, suggesting that the C_3H_6 oxidation takes place at surfaces that have a Mo/Bi ratio of approximately 0.5. Thus, the $\gamma(H)$ -phase likely contains sites that are selective for the C_3H_6 oxidation despite its Mo/Bi of 0.5.

Okamoto et al. [16] reported that the Mo/Bi surface ratio for their $\gamma(L)$ catalyst was 0.54 using an XPS method. Uchida and Ayame [17] reported a Mo/Bi surface ratio for their $\gamma(L)$ catalyst of 0.67 using an XPS method. Soares et al. [8] recently reported a Mo/Bi surface ratio of 0.62 for their $\gamma(L)$ catalyst. These researchers [8,16,17] prepared their $\gamma(L)$ phase catalysts by the method of Batist et al. (i.e., the (A) method described in this work) [12]. Thus, the enrichment in Mo ions at the surface of the $\gamma(L)$ phase should take place in the (A) preparation method, but it does not occur in the (B) preparation method. Burrington and Grasselli [18] reported that their $\gamma(L)$ catalyst had low activity, and it was prepared by what is referred as the (B) method in this work.

3.2. Partial oxidation of C_3H_6 over $\gamma(L)$ - Bi_2MoO_6 catalysts that contain excess MoO_3

Fig. 4 shows the results of C_3H_6 oxidations over the $\gamma(L)$ - Bi_2MoO_6 (C) catalysts as a function of excess in MoO_3 . The selectivities in producing acrolein increased with increases in wt% MoO_3 and reached approximately 86% at 6 wt% MoO_3 with the catalysts prepared by (C) method. The yields also increased with increases in wt% MoO_3 and the conversions of C_3H_6 ranged from 1.4 to 1%. The catalysts in which the Mo/Bi was 0.5 exhibited very low selectivity for the production of acrolein. These catalysts may have different areas but their difference will be small because of the same preparation temperature. The high selectivities of $\gamma(L)$ catalysts with excess Mo likely resulted from the presence of β -phase material as described next section.

The (B) catalysts that were excess in MoO_3 by 2–6 wt% showed 40–50% of acrolein selectivities, which were somewhat smaller than those with the (C) catalysts in Fig. 4. The yields to acrolein formation over the (B) catalysts were also 2–3 times smaller than those over the (C) catalysts although the figure is not shown. These (B) catalysts indicated the structure of $\gamma(L)$ -phase using Raman and XRD methods. These suggest that surface structures of $\gamma(L)$ -phase (B) seem to have smaller Mo enrichment than those of (C) catalysts.

We attempted the C_3H_6 oxidation over the $\gamma(L)$ -phase (B) catalysts that were deficient in MoO_3 by 2–4 wt%. They exhibited very low acrolein selectivities (below 5%) and exhibited 1–3% of conversions of C_3H_6 . These catalysts had $\gamma(L)$ -phase structure in the bulk using Raman spectra. Low oxidation selectivities seem to come from Bi enrichment and Mo deficiency at the surface. The roles of the pure $\gamma(L)$ -phase in determining structural and catalytic behaviors will also be discussed later.

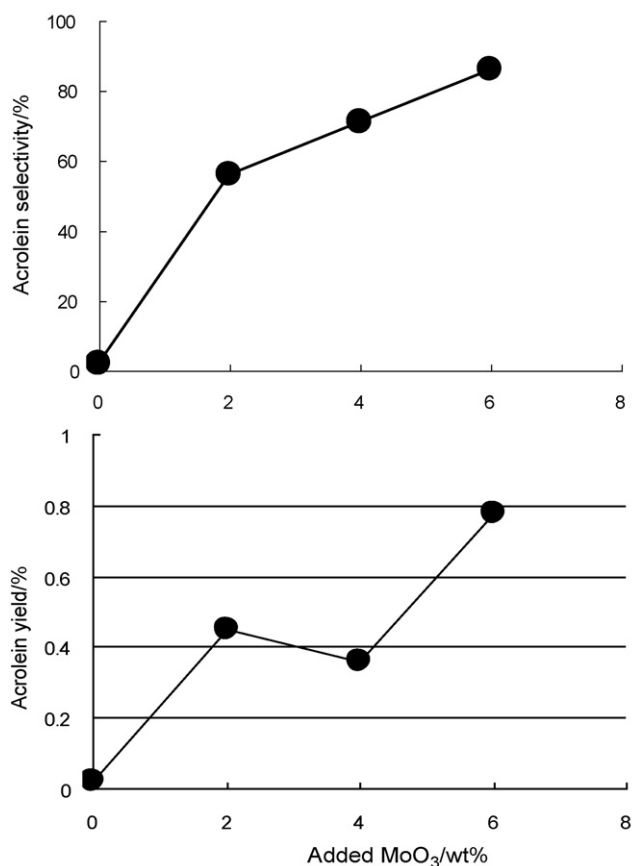


Fig. 4. Yield and selectivity to acrolein in C₃H₆ oxidation over $\gamma(\text{L})\text{-Bi}_2\text{MoO}_6$ (C) catalysts that contained an excess of MoO₃ in the absence of dioxygen. A reading of "0" on the horizontal axis indicates pure $\gamma(\text{L})\text{-Bi}_2\text{MoO}_6$. The catalysts were prepared by the (C) methods (see Section 2.1). Experimental conditions: $P_{\text{C}_3\text{H}_6} = 3$ kPa, 500 °C, reaction time of 5 min, and using 1 g of catalyst.

3.3. Characterization of $\gamma(\text{L})\text{-Bi}_2\text{MoO}_6$ catalysts containing excess MoO₃

The Raman spectrum of the $\gamma(\text{L})\text{-Bi}_2\text{MoO}_6$ catalyst containing 2 wt% excess of MoO₃ is shown in Fig. 5. A small band at 890 cm⁻¹, which is attributed to β -phase material, appeared in the spectra of the (C) catalyst containing a 2 wt% excess of MoO₃. The calculated Mo/Bi should be 0.52 when 2 wt% of MoO₃ are reacted with the whole $\gamma(\text{L})\text{-Bi}_2\text{MoO}_6$ mixed. However, its surface Mo/Bi ratio is 0.67 as shown in the XPS results in Table 3. These suggest that the formation of β -phase material takes place at the surface of the $\gamma(\text{L})\text{-Bi}_2\text{MoO}_6$ phase at 500 °C during the catalyst's preparation. The typical band at 1000 cm⁻¹ for MoO₃ was not detected. The intensity of the band

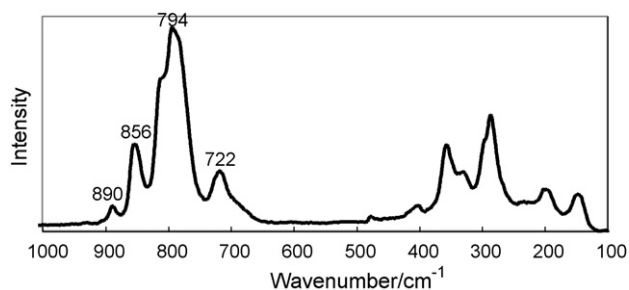


Fig. 5. Raman spectra of $\gamma(\text{L})\text{-Bi}_2\text{MoO}_6$ catalysts prepared using the (C) method. $\gamma(\text{L})\text{-Bi}_2\text{MoO}_6$ + 2 wt% excess MoO₃ heated at 500 °C. The band at 890 cm⁻¹ is assigned to the β -phase. The bands at 856, 794, and 722 cm⁻¹ result from $\gamma(\text{L})\text{-Bi}_2\text{MoO}_6$.

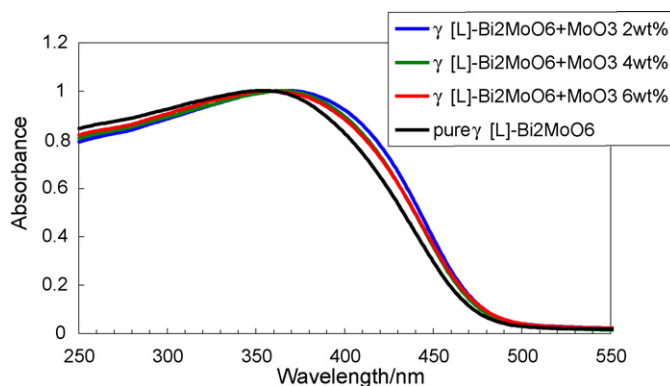


Fig. 6. UV-vis spectra of the $\gamma(\text{L})\text{-Bi}_2\text{MoO}_6 + \text{MoO}_3$ (C) catalysts as a function of MoO₃ content. The MoO₃ is converted to β -phase material as shown in Fig. 5.

at 890 cm⁻¹ increased when the excess of Mo was increased, up to an excess of 6 wt% MoO₃. XPS results indicated that the Mo/Bi surface ratio ranged from 0.49 to 0.73 when 0 to 6 wt% MoO₃ was added (Table 3). These results collectively suggest that the high selectivity for acrolein production in the oxidation of C₃H₆ is a result of $\beta\text{-Bi}_2\text{Mo}_2\text{O}_9$ on the $\gamma(\text{L})\text{-Bi}_2\text{MoO}_6$ phase. Matsuura et al. [3] have previously reported similar results. The XPS results in Table 3 shows that Mo/Bi ratios did not reach 1.0, which indicates that the surfaces were not completely covered with β -phase under these conditions. According to the results of Soares et al. [8], Mo/Bi ratios determined by XPS ranged from 0.62 to 0.86 when considering catalysts with between 100% of $\gamma(\text{L})\text{-Bi}_2\text{MoO}_6$ and 50% $\beta\text{-Bi}_2\text{Mo}_2\text{O}_9$. These results also support the idea that β -phase material is present at the surface and that it is responsible for the partial oxidation of 1-butene.

The UV-vis spectra of β - and $\gamma(\text{L})\text{-Bi}_2\text{MoO}_6$ showed maxima at 360–370 nm [19,20]. In the case of pure $\gamma(\text{L})\text{-Bi}_2\text{MoO}_6$, a band at ca. 410 nm was also observed [20,21]. Fig. 6 shows the UV-vis spectra of $\gamma(\text{L})\text{-Bi}_2\text{MoO}_6$ catalysts prepared by the (C) method as a function of excess MoO₃ content. The bands present can be confidently assigned to $\gamma(\text{L})\text{-Bi}_2\text{MoO}_6$, but do indicate some shouldering on the longer wavelength side of the 410 nm peak. Fig. 7 shows the difference spectra, in which the spectra of pure $\gamma(\text{L})\text{-Bi}_2\text{MoO}_6$ was subtracted from that of the $\gamma(\text{L})\text{-Bi}_2\text{MoO}_6 + \text{MoO}_3$ catalysts where $\beta\text{-Bi}_2\text{Mo}_2\text{O}_9$ has formed at the surface of the pure $\gamma(\text{L})\text{-Bi}_2\text{MoO}_6$. A new band at ca. 430 nm was evident, and this differential band appeared to be shifted from the band at ca. 410 nm. This indicates that the β -phase formed in these catalysts likely interacted with the Mo⁶⁺ ions of $\gamma(\text{L})\text{-Bi}_2\text{MoO}_6$, which caused a red shift in the UV-vis absorption. According to Matsuura et al. [3] β -phase formation seems to occur by the reaction of MoO₃ with the Bi₂O₂ layer of the $\gamma(\text{L})\text{-Bi}_2\text{MoO}_6$.

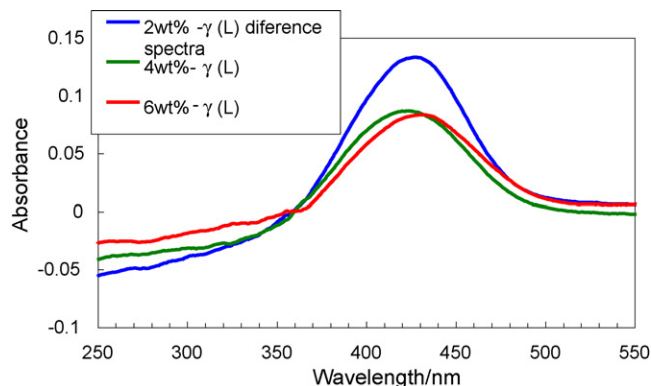


Fig. 7. Difference UV-vis spectra. Spectra of $\gamma(\text{L})\text{-Bi}_2\text{MoO}_6 + \text{MoO}_3$ (wt%) (C) catalysts were subtracted from that of pure $\gamma(\text{L})\text{-Bi}_2\text{MoO}_6$. Difference spectra shows the peak at ca. 430 nm.

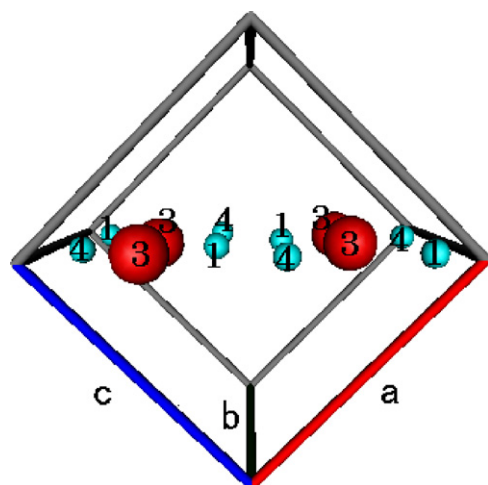


Fig. 8. A visualization of the β - $\text{Bi}_2\text{Mo}_2\text{O}_9$'s crystal structure with oxygen atoms omitted. The small blue spheres (Mo_1 and Mo_4 ions are twin $\beta_1\beta_4$ tetrahedra) and large red spheres (Bi_3 ions) lie in the same plane, i.e., the (101) plane. The other Mo_2 and Mo_3 ions as well as Bi_1 and Bi_2 ions do not lie in the same plane (not shown in the figure). Numerals denote the position numbers of the Mo and Bi atoms as reported by Buttery et al. [10] and Chen and Sleight [15]. The axes are denoted by a, b, and c. (For interpretation of the references to color in this figure legend, the reader is referred to the web version of the article.)

phase. Thus, the new β -phase material seems to grow along b -axis (i.e., perpendicular to MoO_2 – Bi_2O_2 layers of the $\gamma(\text{L})$ phase shown in Fig. 10 (oxygen ions are omitted)). In this case, the interaction between the β -phase and the $\gamma(\text{L})$ phase seems to be limited and weak, since the red shift's intensity did not depend on the amount of excess MoO_3 added (i.e., the red shift intensity did not vary with concentration of β -phase present, as shown in Fig. 7). These results are likely important for understanding the oxygen transfer between the β -phase and the $\gamma(\text{L})$ -phase during the oxidation of C_3H_6 , and will be addressed later.

3.4. Crystal structure visualizations of β -, $\gamma(\text{L})$ -, and $\gamma(\text{H})$ -phases

We previously attempted to determine unique crystal structure characteristics for each of the phases [11]. The crystal structure visualizations indicated that the α -phase consists of $\alpha_1\alpha_1$ and $\alpha_2\alpha_3$ twin tetrahedral structures, and that the Mo ions are nearly in the same plane as the Bi ions, which demonstrated in Ref. [11]. Fig. 8 shows the (101) plane of the β - $\text{Bi}_2\text{Mo}_2\text{O}_9$ crystal lattice (oxygen ions removed), where the twin Mo tetrahedral structure $\beta_1\beta_4$ is present, and the Mo and Bi_3 ions lie in the same plane. The β -phase also has $\beta_2\beta_3$ twin Mo tetrahedral structures, but their Mo and Bi ions do not lie in the same plane (not shown in the figures). Fig. 9 shows a crystal structure visualization of the $\gamma(\text{H})$ - Bi_2MoO_6 structure with oxygen ions removed. As reported by Buttery et al. [10], it has γ_1 , γ_2 , γ_3 , and γ_4 Mo tetrahedra, which exist as $\gamma_2\gamma_3$, $\gamma_1\gamma_1$, and $\gamma_4\gamma_4$ twin structures. As indicated in the figure, the twin $\gamma_2\gamma_3$ structure (shown with oxygen ions removed) is present in the middle of the unit cell, and is surrounded by six Bi ions. These Mo_2 , Mo_3 , and Bi ions are nearly in the same plane. However, the Mo_1 and Mo_4 ions as well as the Bi ions do not lie in the same plane. Fig. 10 shows a visualization of two unit cells of the $\gamma(\text{L})$ -phase with oxygen ions removed. Real unit cells of the $\gamma(\text{L})$ - Bi_2MoO_6 material consist of MoO_2 and Bi_2O_2 layers along the b -axis, and Mo and oxygen ions exist as distorted octahedral structure [14]. This material does not contain a twin Mo tetrahedral structure, and the Mo ions do not lie in the same plane as the Bi ions. Thus, α -, β -, and $\gamma(\text{H})$ -phase as well as Mo rich (surface β -phase) $\gamma(\text{L})$ -phase catalysts, which are selective catalysts, have twin Mo tetrahedral structure sites and their Mo and Bi ions lie in the same plane. While,

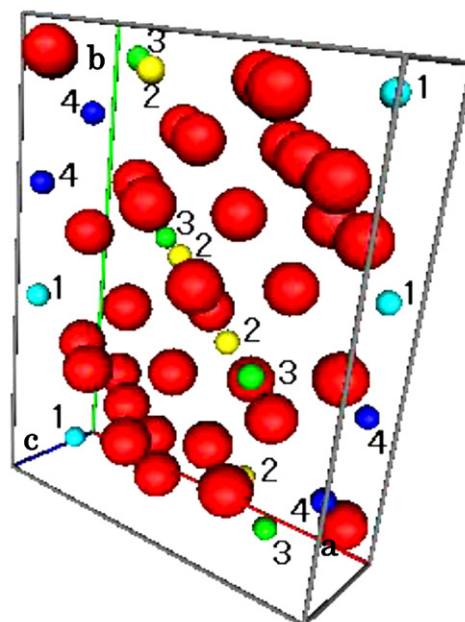


Fig. 9. A visualization of the $\gamma(\text{H})$ - Bi_2MoO_6 crystal structure with oxygen atoms omitted. Two twin $\gamma_2\gamma_3$ tetrahedra (Mo_2 and Mo_3 ions) and 6 Bi ions lie in the same plane. Small spheres denote Mo ions, while large red spheres denote Bi ions. Numerals denote the position numbers of the Mo and Bi atoms as reported by Buttery et al. [10]. The axes are denoted by a, b, and c. (For interpretation of the references to color in this figure legend, the reader is referred to the web version of the article.)

the pure $\gamma(\text{L})$ -phase, which is less selective catalyst, has no such structures.

By employing deuterated propene and microwave spectroscopy techniques, we previously reported and proposed that a rapid equilibration between the π -allyl and the σ -allyl species occurs on the Mo ions of the α -phase [22]. In a quantum chemical study, Anderson et al. [23] reported that the $\text{Bi}_2\text{Mo}_3\text{O}_{20}^{12-}$ cluster model system

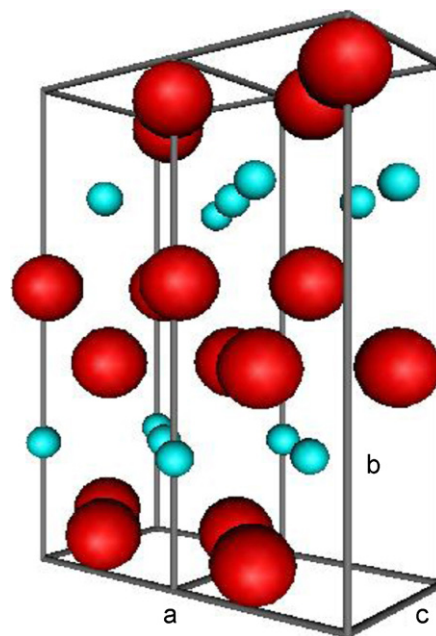


Fig. 10. A visualization of two unit cells of the $\gamma(\text{L})$ - Bi_2MoO_6 koechlinite (JCPDS 21-102) [14] with oxygen atoms omitted. Small blue spheres denote Mo ions, while large red spheres denote Bi ions. a, b, and c denote the axes. The Mo and Bi ions do not lie in the same plane. (For interpretation of the references to color in this figure legend, the reader is referred to the web version of the article.)

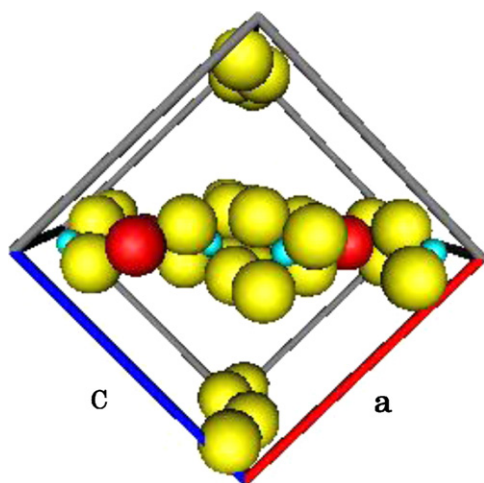


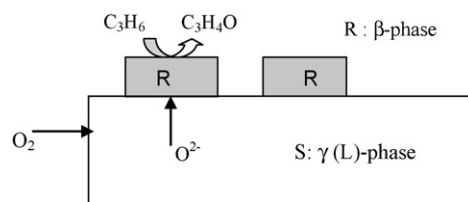
Fig. 11. A visualization of the (101) plane of the β - $\text{Bi}_2\text{Mo}_2\text{O}_9$ including the oxygen ions (yellow). Oxygen ions have been added shown in Fig. 8. Four sets of twin $\beta_1\beta_4$ tetrahedra, Mo_1 and Mo_4 ions, as well as Bi_3 ions lie in the same plane. (For interpretation of the references to color in this figure legend, the reader is referred to the web version of the article.)

chosen to study the reaction's mechanism contain all the cations in a single plane, and that it is bulk superimposable. Fig. 11 shows the (101) plane of the β -phase (including oxygen ions, which were omitted in Fig. 8). All of the steps from hydrogen abstraction to $\text{CH}_2=\text{CH}-\text{CHO}$ formation can proceed at these sites (i.e., the (101) plane of β -phase), but re-oxidation cannot. These sites must be exposed at the surface for selective oxidation to occur, and some of the oxygen ions are likely released by the reaction with the π -allyl species.

3.5. Roles of $\gamma(\text{L})$ - Bi_2MoO_6 phase in the oxidation as determined by ^{18}O tracer and a modified redox mechanism in C_3H_6 oxidation

There have been many reports that oxygen ions of $\gamma(\text{L})$ -phase are responsible for C_3H_6 oxidation. Hoefs et al. previously reported that the fraction of oxygen atoms exchanged with ^{18}O during the partial oxidation of C_3H_6 increased in the order $\gamma > \beta > \alpha$ -phase. This was determined using IR and Raman spectroscopy [24]. Additionally, Krenzke and Keulks reported that the percentage of oxygen atoms on these catalysts that participated during oxidation was 100% for γ -phase material, but only 2–9% for α -phase material [25]. According to these reports, the selectivity for the production of acrolein when reactions were carried out over γ -phase was above 90%. Krenzke and Keulks reported [26] that the γ -phase material prepared by their method was very active in the partial oxidation of C_3H_6 . It seems that the initial high activity and selectivity of their γ -phase material resulted from surface Mo enrichment. The $\gamma(\text{L})$ -phase plays an important role in the re-oxidation because 100% of the lattice oxygen ions are reported to participate in this step [25]. We reported previously [12], that the catalyst's oxygen atoms of $\gamma(\text{L})$ - $\text{Bi}_2\text{MoO}_6/\text{SiO}_2$ catalyst ($\text{Mo}/\text{Bi} = 0.52$, with a 4% excess of Mo ions) were exchanged by C_3H_6 followed by re-oxidation with $^{18}\text{O}_2$. The Raman bands from the $\gamma(\text{L})$ -phase were shifted to lower wave numbers as the amount of ^{18}O exchange increased, while the band at 885 cm^{-1} from the β -phase material changed less, which indicates the oxygen atoms are inserted at the $\gamma(\text{L})$ -phase preferentially.

A modified redox mechanism was proposed [27] in which the reduction of oxide catalyst by C_3H_6 and the re-oxidation by O_2 occur at different regions of the Bi–Mo oxide surface. We reported [27] that the catalyst ($\text{Mo}/\text{Bi} = 1$, β -phase (major)) exhibited high activity and high acrolein selectivity in C_3H_6 oxidation. This work over



Scheme 1. Model of C_3H_6 oxidation over $\gamma(\text{L})$ - Bi_2MoO_6 + surface β - $\text{Bi}_2\text{Mo}_2\text{O}_9$ catalyst. R: the sites for partial oxidation of C_3H_6 . S: the sites for re-oxidation from gas phase O_2 .

Mo rich $\gamma(\text{L})$ -phase catalyst suggests that C_3H_6 reacts with the oxide ions in the R region (e.g. (101) plane of β -phase) and as a result the acrolein seems to form on those sites, as shown in Scheme 1. The insertion of oxygen at anion vacancies (S) appears to take place at the $\gamma(\text{L})$ -phase (i.e., anion vacancies in MoO_2 layer). According to Krenzke and Keulks [25] the reaction is first order in C_3H_6 and zero order in O_2 above 400°C . This suggests that the re-oxidation step is very rapid when compared to the reduction step. This scenario requires that anion vacancies be produced at the $\gamma(\text{L})$ -phase as soon as the oxidation takes place at β -phase. It also requires that anion vacancies or oxygen ions be transferred very rapidly between the β -phase and the $\gamma(\text{L})$ -phase. The fact that the β -phase grows perpendicular to the MoO_2 - Bi_2O_2 layers may make it possible for such a rapid oxygen transfer to occur. The rapid transfer of anion vacancies or oxygen ions also needs to occur in the bulk $\gamma(\text{L})$ -phase. This movement of anion vacancies or oxygen ions may be possible along the MoO_2 layers during the partial oxidation reaction, though more studies will be needed to confirm this.

4. Conclusion

Pure $\gamma(\text{L})$ - Bi_2MoO_6 exhibited poor selectivity in the partial oxidation of C_3H_6 to acrolein. However, the Mo enriched $\gamma(\text{L})$ -phase catalyst exhibited good selectivity. Furthermore, pure $\gamma(\text{H})$ - Bi_2MoO_6 exhibited a high selectivity for acrolein formation. The amount of excess MoO_3 added to $\gamma(\text{L})$ - Bi_2MoO_6 was found to be directly correlated with β - $\text{Bi}_2\text{Mo}_2\text{O}_9$ formation during the preparation process. This β -phase appeared to be in contact with the $\gamma(\text{L})$ -phase, and provided high selectivity for acrolein production in the partial oxidation of C_3H_6 . β -Phase material seemed to grow in the direction to the b -axis of $\gamma(\text{L})$ -phase (i.e., in the perpendicular to the MoO_2 - Bi_2O_2 layers). Crystal structure visualization revealed that α -, β -, and $\gamma(\text{H})$ -phases have twin Mo tetrahedral structures, and that their Mo and Bi ions lie in the same plane, while the $\gamma(\text{L})$ -phase has no similar structures. The high activities and peculiar kinetics of the Mo rich $\gamma(\text{L})$ -phase catalysts can be explained by the separation of reduction and re-oxidation sites. The re-oxidation sites at $\gamma(\text{L})$ -phase have a very important role in the insertion of oxygen from the gas phase. According to this mechanism, a very rapid transfer of oxygen ions and vacancies between the β -phase and the pure $\gamma(\text{L})$ -phase should be needed to achieve the partial oxidation of C_3H_6 .

Acknowledgements

The authors thank Prof. Hashimoto and Dr. Myo for the XSP measurements, as well as Prof. Endo and Prof. Kim for the laser Raman spectral measurements at the Department of Electrical and Electronic Engineering, Faculty of Engineering, Shinshu University.

References

- [1] R.K. Grasselli, J.D. Burrington, Adv. Catal. 30 (1981) 133–162.
- [2] T.P. Snyder, C.G. Hill Jr., Catal. Rev. Sci. Eng. 31 (1989) 43–95.
- [3] I. Matsuura, R. Shut, K. Hirakawa, J. Catal. 63 (1980) 152–166.

- [4] N. Song, C. Rhodes, J.K. Bartley, S.H. Taylor, D. Chadwick, G.J. Hutchings, *J. Catal.* 236 (2005) 282–291.
- [5] M.T. Le, W.J.M. van Well, P. Stoltze, I. van Drissche, S. Hoste, *Appl. Catal. A* 282 (2005) 189–194.
- [6] A. Ayame, K. Uchida, M. Iwataya, M. Miyamoto, *Appl. Catal. A* 227 (2002) 7–17.
- [7] W.J.M. van Well, M.T. Le, N.C. Schiødt, S. Hoste, P. Stoltze, *J. Mol. Catal. A* 256 (2006) 1–8.
- [8] A.P.V. Soares, L.D. Dimitrov, M.C.A. Oliveira, L. Hilaire, M.F. Portela, R.K. Grasselli, *Appl. Catal. A: Gen.* 253 (2003) 191–200.
- [9] D.J. Buttrey, D.A. Jefferson, J.M. Thomas, *Philos. Mag. A* 53 (1986) 897–906.
- [10] D.J. Buttrey, T. Vogt, U. Wildgruber, W.R. Robinson, *J. Solid. State Chem.* 111 (1994) 118–127.
- [11] T. Ono, K. Utsumi, M. Kataoka, Y. Tanaka, F. Noguchi, *Catal. Today* 91–92 (2004) 181–184.
- [12] T. Ono, N. Ogata, *J. Chem. Soc. Faraday Trans.* 90 (1994) 2113–2118.
- [13] Ph.A. Batist, J.F.H. Bouens, G.C.A. Schuit, *J. Catal.* 25 (1972) 1–11.
- [14] A.F. van den Elzen, G.D. Rieck, *Acta Cryst. B* 29 (1973) 2436–2438.
- [15] H.Y. Chen, A.W. Sleight, *J. Solid State Chem.* 63 (1986) 70–75.
- [16] Y. Okamoto, F. Morikawa, J. Degawa, T. Imanaka, S. Teranishi, *Chem. Lett.* (1983) 1853–1856.
- [17] K. Uchida, A. Ayame, *J. Surf. Sci. Soc. (in Japanese)* 15 (1994) 393–399.
- [18] J.D. Burrington, R.L. Grasselli, *J. Catal.* 59 (1979) 79–99.
- [19] P.C.H. Mitchell, F. Trifiro, *J. Chem. Soc. A* (1970) 3183–3188.
- [20] G. Blasse, L. Boon, *Ber. Bunsenges. Phys. Chem.* 88 (1984) 929–930.
- [21] R. Olier, G. Coudurier, M. El Jamal, M. Forissier, J.C. Vedrine, *J. Chem. Soc. Faraday Trans. 1* 85 (1989) 2615–2624.
- [22] T. Ono, N. Ogata, R.L. Kuczkowski, *J. Catal.* 175 (1998) 185–193.
- [23] A.B. Anderson, D.W. Ewing, Y. Kim, R.L. Grasselli, J.D. Burrington, J.F. Bradzil, *J. Catal.* 96 (1985) 222–233.
- [24] E.V. Hoefs, J.R. Monnier, G.W. Keulks, *J. Catal.* 57 (1979) 331–337.
- [25] L.D. Krenzke, G.W. Keulks, *J. Catal.* 61 (1980) 316–325.
- [26] L.D. Krenzke, G.W. Keulks, *J. Catal.* 64 (1980) 295–302.
- [27] T. Ono, T. Nakajyo, T. Hironaka, *J. Chem. Soc. Faraday Trans.* 86 (1990) 4077–4081.